Time-domain vs frequency-domain identification for a small-scale helicopter

Meiliwen Wu and Marco Lovera

Abstract In this work the problem of model identification for the fight dynamics of a small scale helicopter is considered. Two model identification methods, a time-domain subspace identification method and a frequency-domain output-error one, are evaluated and compared in detail in terms of time-domain simulations and in frequency response analyses. Results show that both methods can predict the time-domain responses in good agreement with the flight test results, with relative advantages and disadvantages which are discussed in detail.

1 Introduction

In recent years, the problem of system identification (SI) of small-scale helicopter dynamics has been studied extensively. Indeed, there has been seen a significant growth for the application of small-scale helicopters, such as crop dusting, remote sensing, search and rescue, goods delivery and many other. Small-scale helicopters have a high maneuverability, which guarantees a good dynamic performance even in aerobatic flight motions. Based on these application demands, and in view of the problem of tuning high-performance control laws, accurate identified dynamic models are essential for this kind of helicopters.

Unlike full-scale helicopters, for small-scale ones carefully modeling according to first principles does not guarantee an accurate model predicting the whole-envelope dynamic behavior. Nonlinear modeling is challenging because of their different designs and low-Reynolds aerodynamics. Looking at previous modeling experiences of small-scale helicopters, from heavier weight to the light, there are

Meiliwen Wu
Politecnico di Milano, e-mail: meiliwen.wu@polimi.it

Marco Lovera
Politecnico di Milano, e-mail: marco.lovera@polimi.it

several classical research platforms: 10 kg $\sim$ 100 kg: Yamaha R-50[1], AF25B[2]; 5 kg $\sim$ 10kg: MIT X-cell[3,4,5], Evolution-EX[6], NUS Raptor 90 SE HeLion[7]; 1 kg $\sim$ 5 kg: Raptor 50[8]; micro range below 1kg: HoneyBee[9], *etc.*. Although the methods and dynamic features of the listed researches vary, there are some common points. First, a simple but accurate model is always a desired objective. The modeling may begin from first principles, but ends in all cases with a model order no more than 13^{th}, which always contains the rigid body dynamics, rotor flap dynamics, and stabilizer bar dynamics. Second, the frequency-domain and time-domain analysis are essential in the process. A combination of the two is becoming a trend for getting more information from the flight data.

In frequency-domain rotorcraft SI, linear model identification has become a standardized procedure, typically realized by the software package CIFER[1,10]. In CIFER, the time-domain flight data is used to estimate frequency response functions and the corresponding coherence function to identify Single-Input Single-Output (SISO) or Multiple-Input Multiple-Output (MIMO) models. The method removes noise and extracts frequency-domain information in a computationally efficient way. However, the method is established based on iterative calculation. The initial settings will influence the iteration results greatly, which will be an engineering problem when dealing with a complex unknown model. The windowing and averaging procedures that perform Fourier transform and estimation should also be carefully selected. Additionally, the CIFER method can only analyze linear models; for nonlinear model identification, the method will not be suitable.

Apart from the frequency-domain identification mainly by CIFER, time-domain identification has more classifications, such as the maximum likelihood (ML) estimator, prediction error method (PEM), subspace method, *etc.*. Specially, Subspace Model Identification (SMI) methods[11] have been proven extremely successful in dealing with complex MIMO system such as helicopters. SMI algorithms works in a very natural and noniterative way when dealing with MIMO models and the involved computations can be carried out in a numerically stable and efficient way without needing to consider the initial values and windowing structure like in CIFER. About two decades ago, only SMI algorithms such as MOESP (Multivariable Output Error State Space) and bootstrap-based[12,13,14,15] were considered. The latest developments of SMI method have not been well exploited, such as the unbiased model estimation from data collected under controlled feedback, or continuous-time models using Lagrange-based data transformations. Preliminary results have been obtained using predictor-based SMI (see, *e.g.*,[16,17,18]). PBSID$_{opt}$ differs from the original PBSID algorithm in the computation of the predictors. In the optimized algorithm, the estimation of the predictors is formulated as a weighted least squares problem. PBSID$_{opt}$ is proofed to be asymptotically efficient in a number of examples[19].

This study compares a frequency-domain method (CIFER) with a time-domain method (PBSID$_{opt}$) of SI in extracting the coupled roll/pitch linear model in hover condition on an 8.1 kg small-scale helicopter. The paper is organized as follows: Section 2 introduces the problem and explains the data collection. Section 3 shows the two approaches from frequency domain and time domain respectively. Section 4

presents the identification results and validations. In Section 5, the main conclusions are given.

2 Problem statement and data illustration

In this work, the identification dataset was acquired on an 8.1 kg small-scale single-rotor JR700 helicopter (Figure 1). The main parameters of JR700 compared with three similar small-scale helicopters are shown in Table 1. This helicopter did not install any mechanical augmentation component (*e.g.*, the stabilizer bar), whereas a 3-axis gyro (CGY750) was embedded to stabilize the longitudinal, lateral, and yaw dynamics. On the helicopter, the onboard computer was used to record the input control signals and the output responses, *e.g.*, angular velocities, accelerations, attitude angles, *etc.* (see Figure 2). For extracting the coupled roll/pitch linear model, flight tests of sweep motions were manually conducted on lateral and longitudinal channels in hover by a pilot. For identification purposes each dataset is defined by

$$\begin{cases} u = [\delta_{lon}, \delta_{lat}]^T \\ y = [\theta, \phi, q, p]^T, \end{cases} \tag{1}$$

where u represents the input signal of two-direction cyclic pitches (normalized to [-0.5,0.5]) and y contains the two-direction Euler angles and angular velocities. A total of 9 sets of best sweep-motion flight data are selected for identification. Data sets have durations of 15 s or 30 s. Additionally, 2 more sets of flight data are used for validation.

Figure 1. The small-scale helicopter JR700.

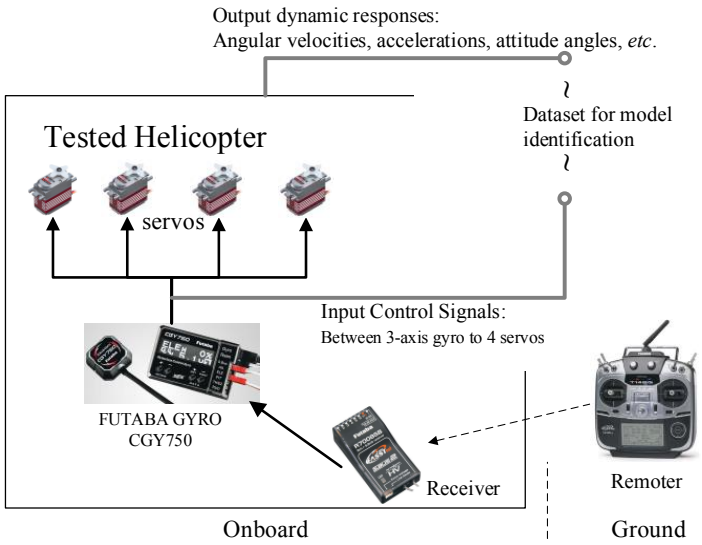

Figure 2. Data collection illustration.

Table 1. JR700 physical parameters compared with three similar helicopters

Parameters	JR700	Raptor 50 [8]	X-cell [1]	HeLion [7]
Gross weight (kg)	8.1	4.8	8.15	9.75
Rotor solidity	0.052	0.05	0.05	0.055
Blade inertia $(kg \cdot m^2)$	0.04	0.035	0.02	0.055
Main rotor diameter (cm)	153.4	134.37	152.4	141
Rotor speed (rad/s)	178	191	167	193.73

3 Approach

In this section some background on the methods and tools employed in this study is provided. Specifically, as for frequency-domain identification a grey-box model approach has been adopted, in the first subsection the model structure for the flight dynamics of the small-scale helicopter under study is also presented.

3.1 Frequency-domain method: CIFER

In order to better select the order of the model, the dynamic features of the coupled roll/pitch model should be checked in advance.

The helicopter as a whole can be regarded as a 6-DoF rigid body system[20]. According to Newton-Euler equations,

$$\begin{cases} \dot{v} = \dfrac{1}{m}F - \omega \times v \\ \dot{\omega} = I^{-1}M - I^{-1}(\omega \times I\omega) \\ \dot{\Theta} = \Phi(\Theta)\omega, \end{cases} \tag{2}$$

where v is the linear velocity vector, ω is the angular velocity vector, and Θ is the vector of Euler angles. F and M are the external force and moment vectors. I is the matrix of moment of inertia. Φ is the velocity transformation matrix.

Additionally, the small-scale helicopter has a considerable high-frequency of motion, so the high-frequency features of the main rotor dynamics cannot be neglected. The flapping dynamics of the rotor can be expressed as quasi-steady coupled first-order tip-path-plane equations[1],

$$\begin{cases} \tau_f \dot{a} = -a - \tau_f q + A_b b + A_{\delta_{lon}}\delta_{lon} + A_{\delta_{lat}}\delta_{lat} \\ \tau_f \dot{b} = -b - \tau_f p + A_b a + B_{\delta_{lon}}\delta_{lon} + B_{\delta_{lat}}\delta_{lat}, \end{cases} \tag{3}$$

where a and b are the longitudinal and lateral flapping angles, τ_f is the rotor time constant, A_b, $A_{\delta_{lat}}$ and $B_{\delta_{lon}}$ are the coupling parameters and $A_{\delta_{lon}}$, $A_{\delta_{lat}}$, $B_{\delta_{lon}}$, and $B_{\delta_{lat}}$ are the maneuver coefficients. Finally, considering the 2 states corresponding to the flapping dynamics, an order 6m coupled roll/pitch, dynamic model is studied. The state space model can be expressed as

$$\begin{aligned} \dot{x} &= Ax + Bu_\tau(t) \\ y &= Cx + Du_\tau(t), \end{aligned} \tag{4}$$

where the state is $x = [\theta, \phi, q, p, a, b]^T$ and $u_\tau(t) = \left[\delta_{lon}(t-\tau_{lon})\ \ \delta_{lat}(t-\tau_{lat})\right]^T$ is the delay vector. According to the above dynamic analysis, the equations can be expanded as

$$\begin{bmatrix} \dot{\theta} \\ \dot{\phi} \\ \dot{q} \\ \dot{p} \\ \dot{a} \\ \dot{b} \end{bmatrix}(t) = \begin{bmatrix} 0 & 0 & 1 & 0 & 0 & 0 \\ 0 & 0 & 0 & 1 & 0 & 0 \\ 0 & 0 & 0 & 0 & M_a & 0 \\ 0 & 0 & 0 & 0 & 0 & L_b \\ 0 & 0 & -1 & 0 & -1/\tau_f & A_b/\tau_f \\ 0 & 0 & 0 & -1 & A_b/\tau_f & -1/\tau_f \end{bmatrix} \begin{bmatrix} \theta \\ \phi \\ q \\ p \\ a \\ b \end{bmatrix}(t) + \begin{bmatrix} 0 & 0 \\ 0 & 0 \\ 0 & 0 \\ 0 & 0 \\ A_{\delta_{lon}}/\tau_f & A_{\delta_{lat}}/\tau_f \\ B_{\delta_{lon}}/\tau_f & B_{\delta_{lat}}/\tau_f \end{bmatrix} \begin{bmatrix} \delta_{lon}(t-\tau_{lon}) \\ \delta_{lat}(t-\tau_{lat}) \end{bmatrix} \tag{5}$$

$$\begin{bmatrix} \theta \\ \phi \\ q \\ p \end{bmatrix}(t) = \begin{bmatrix} 1\,0\,0\,0\,0\,0 \\ 0\,1\,0\,0\,0\,0 \\ 0\,0\,1\,0\,0\,0 \\ 0\,0\,0\,1\,0\,0 \end{bmatrix} \begin{bmatrix} \theta \\ \phi \\ q \\ p \\ a \\ b \end{bmatrix}(t). \tag{6}$$

As for the system identification procedure, in the frequency domain, the Fourier transforms of the input and output data ($[U(j\omega), Y(j\omega)]$) can be related by a frequency-response function $H(j\omega)$:

$$Y(j\omega) = H(j\omega)U(j\omega) \tag{7}$$

which can also be expressed as a combination of magnitude and phase:

$$H(j\omega) = |H(j\omega)|e^{-j\phi(j\omega)}. \tag{8}$$

The magnitude and phase expressions are commonly used in frequency-domain analysis. For a MIMO system, H is a matrix, relating to different inputs and outputs. The complex frequency-response function relates the input auto-spectral density function $G_{uu}(j\omega)$ with the input-output cross-spectral density function $G_{uy}(j\omega)$.

$$H(j\omega) = G_{uu}^{-1}(j\omega)G_{uy}(j\omega). \tag{9}$$

Then, the coherence function is defined as[10],

$$\gamma_{yu}^2 = \frac{|G_{yu}|^2}{G_{uu}G_{yy}} \leq 1 \tag{10}$$

and a minimum value of 0.6 for γ^2 is used as the lower limit in CIFER. At γ^2 lower than 0.6, the random error of the frequency responses will be too high and the flight data analysis results will not be reliable.

The cost function in CIFER has the general form

$$J(\Theta) = \sum \varepsilon(\omega,\Theta)^T W(\omega)\varepsilon(\omega,\Theta) \tag{11}$$

where ε is the vector of magnitude and phase errors. The weight function W adopts the coherence function. The cost value quantifies the matching quality. The smaller the cost value, the higher the matching degree in frequency domain. According to CIFER, a cost value lower than 100 can reflect a good quality of the identification results. The cost function should be lowered as much as possible. In MIMO identification, CIFER makes use of FRESPID, MISOSA, COMPOSITE and DERIVID panels.

3.2 Time-domain method: predictor-based subspace model identification (PBSID$_{opt}$)

As illustrated in[21], PBSID is a time-domain subspace model identification algorithm with the ability of dealing with data generated in closed-loop. It belongs to the class of black-box methods: it allows to determine dynamics model of a system using only the input-output data gathered in the identification experiments. The obtained model is unstructured, namely with a non-physically motivated state space. Furthermore, since PBSID is a SMI algorithm, it is a non-iterative method: it can be implemented with numerically stable and efficient tools from numerical linear algebra and it has proved to be extremely successful in dealing with the estimation of state-space models MIMO systems in a number of rotorcraft applications (see[18,22]).

The PBSID algorithm, which is briefly described in the following, considers the finite dimensional, LTI state space model class

$$\begin{aligned} x(k+1) &= Ax(k)+Bu(k)+w(k) \\ \tilde{y}(k) &= Cx(k)+Du(k)+\nu(k) \end{aligned} \tag{12}$$

where $x(k) \in \mathbb{R}^n$, $u(k) \in \mathbb{R}^m$, $\tilde{y}(k) \in \mathbb{R}^p$ and $\{\nu(k), w(k)\}$ are ergodic sequences of finite variance satisfying

$$E[\begin{bmatrix} w(t) \\ \nu(t) \end{bmatrix} \begin{bmatrix} w(s)^T & \nu(s)^T \end{bmatrix}] = \begin{bmatrix} Q & S \\ S^T & R \end{bmatrix} \delta_{s,t},$$

with $\delta_{s,t}$ denoting the Kronecker delta function, possibly correlated with the input $u(k)$.

Let now $z(k) = \begin{bmatrix} u^T(k) & y^T(k) \end{bmatrix}^T$ and $\bar{A} = A - KC$, $\bar{B} = B - KD$, $\widetilde{B} = \begin{bmatrix} \bar{B} & K \end{bmatrix}$, where K is the Kalman gain associated with (12), and note that system (12) can be written as

$$\begin{aligned} x(k+1) &= \bar{A}x(k)+\widetilde{B}z(k) \\ y(k) &= Cx(k)+Du(k)+e(k), \end{aligned} \tag{13}$$

where e is the innovation vector. The data equations for the PBSID algorithm can be then derived by noting that propagating $p-1$ steps forward the first of equations (13), where p is the so-called past window length, one gets

$$\begin{aligned} x(k+2) &= \bar{A}^2 x(k) + \begin{bmatrix} \bar{A}\widetilde{B} & \widetilde{B} \end{bmatrix} \begin{bmatrix} z(k) \\ z(k+1) \end{bmatrix} \\ &\vdots \\ x(k+p) &= \bar{A}^p x(k) + \mathscr{K}^p Z^{0,p-1} \end{aligned} \tag{14}$$

where

$$\mathscr{K}^p = \left[\bar{A}^{p-1}\widetilde{B}_0 \ \dots \ \widetilde{B}\right] \tag{15}$$

is the extended controllability matrix of the system and

$$Z^{0,p-1} = \begin{bmatrix} z(k) \\ \vdots \\ z(k+p-1) \end{bmatrix}.$$

Under the considered assumptions, $\bar{A}$ represents the dynamics of the optimal one-step ahead predictor for the system, so the term $\bar{A}^p x(k)$ is negligible for sufficiently large values of p and we have that

$$x(k+p) \simeq \mathscr{K}^p Z^{0,p-1}.$$

As a consequence, the input-output behaviour of the system is approximately given by

$$\begin{aligned} y(k+p) &\simeq C\mathscr{K}^p Z^{0,p-1} + Du(k+p) + e(k+p) \\ &\vdots \\ y(k+p+f) &\simeq C\mathscr{K}^p Z^{f,p+f-1} + Du(k+p+f) + \\ &\quad + e(k+p+f), \end{aligned} \tag{16}$$

so that, introducing the matrix notation defined in the previous subsection, the data equations are given by

$$\begin{aligned} X^{p,f} &\simeq \mathscr{K}^p \bar{Z}^{p,f} \\ Y^{p,f} &\simeq C\mathscr{K}^p \bar{Z}^{p,f} + DU^{p,f} + E^{p,f}. \end{aligned} \tag{17}$$

Considering $p = f$, estimates for the matrices $C\mathscr{K}^p$ and D are first computed by solving the least-squares problem

$$\min_{C\mathscr{K}^p, D} \|Y^{p,p} - C\mathscr{K}^p \bar{Z}^{p,p} - DU^{p,p}\|_F. \tag{18}$$

Defining now the extended observability matrix Γ^p as

$$\Gamma^p = \begin{bmatrix} C \\ C\bar{A} \\ \vdots \\ C\bar{A}^{p-1} \end{bmatrix} \tag{19}$$

and noting that the product of Γ^p and $\mathscr{K}^p$ can be written as

$$\Gamma^p \mathscr{K}^p \simeq \begin{bmatrix} C\bar{A}^{p-1}\widetilde{B} \ldots & C\widetilde{B} \\ 0 & \ldots \quad C\bar{A}\widetilde{B} \\ \vdots & \\ 0 & \ldots C\bar{A}^{p-1}\widetilde{B} \end{bmatrix}, \tag{20}$$

such product can be computed using the estimate $\widehat{C\mathscr{K}^p}$ of $C\mathscr{K}^p$ obtained by solving the least squares problem (18). Recalling now that $X^{p,p} \simeq \mathscr{K}^p \bar{Z}^{p,p}$ it also holds that $\Gamma^p X^{p,p} \simeq \Gamma^p \mathscr{K}^p \bar{Z}^{p,p}$. Therefore, computing the SVD $\Gamma^p \mathscr{K}^p \bar{Z}^{p,p} = U\Sigma V^T$ an estimate of the state sequence can be obtained as $\widehat{X}^{p,p} = \Sigma_n^{1/2} V_n^T = \Sigma_n^{-1/2} U_n^T \Gamma^p \mathscr{K}^p \bar{Z}^{p,p}$, from which, in turn, an estimate of C can be computed by solving the least squares problem

$$\min_C \|Y^{p,p} - \widehat{D}U^{p,p} - C\widehat{X}^{p,p}\|_F. \tag{21}$$

The final steps consist of the estimation of the innovation data matrix $E_N^{p,f}$

$$E_N^{p,f} = Y^{p,p} - \widehat{C}\widehat{X}^{p,p} - \widehat{D}U^{p,p} \tag{22}$$

and of the entire set of the state space matrices for the system, which can be obtained by solving the least squares problem

$$\min_{A,B,K} \|\widehat{X}^{p+1,p} - A\widehat{X}^{p,p-1} - BU^{p,p-1} - KE^{p,p-1}\|_F. \tag{23}$$

4 Results and discussions

4.1 Frequency domain results

The valid frequency ranges ($\gamma^2 \geq 0.6$) of the flight data are shown in Table 2. There are 6 evaluation channels, 4 main-axis responses: $[\delta_{lon}/q,\ \delta_{lon}/\theta,\ \delta_{lat}/p,\ \delta_{lat}/\phi]$ and 2 off-axis responses: $[\delta_{lon}/p, \delta_{lat}/q]$. As shown in the data, main-axis responses have high coherence up to 30 rad/s. However, the coherence in off-axis responses is limited.

The identification results of CIFER are presented in Table 3, utilizing the coupled roll/pitch model in equations (5) and (6). Among the identified parameters, there is one rotor aerodynamic parameter τ_f, two aerodynamic derivatives $[M_a, L_b]$, two main-axis maneuver coefficients $[A_{\delta_{lon}}, B_{\delta_{lat}}]$, and several off-axis parameters. In the table, all of the percentage Cramer-Rao bounds (CR% in the table) of the parameter estimates are lower than 20%, and the insensitivity is quite low. The average cost function of the coupled roll/pitch model is 41.5.

The frequency results compared with the nonparametric frequency response functions of flight data are shown in Figure 3. In the main-axis, the magnitude pre-

dictions match well with the flight responses, while the phase predictions present some errors in high-frequency above 10 rad/s. The coherence of channels $[\delta_{lon}/\theta, \delta_{lat}/\phi]$ are slightly lower than that of channels $[\delta_{lon}/q, \delta_{lat}/p]$. Indeed, the quality of angular velocity predictions dominates the identification performance on this coupled roll/pitch model. Figures 3c and 3d show the off-axis results. A lower matching degree is discovered in these off-axis predictions compared with the main-axis, considering the relative low coherence and short frequency range of these channels. In general, CIFER gives a good quality model in predicting the frequency responses of the flight data.

Table 2. Frequency ranges (rad/s) in CIFER.

	δ_{lon}	δ_{lat}
q	1.9 - 27	1.9 - 6.5
p	1.9 - 10	1.9 - 35
θ	1.9 - 15	-
ϕ	-	1.9 - 31

Table 3. Identified parameters in hover from CIFER.

Parameters	Value	CR [%]	Insensitivity [%]
τ_f	0.05136	6.934	0.8350
M_a	348.4	8.341	1.871
L_b	721.7	5.466	1.787
A_b	0.5133	5.725	2.485
$A_{\delta_{lat}}$	0.0721	8.372	2.371
$A_{\delta_{lon}}$	0.4505	6.870	1.240
$B_{\delta_{lat}}$	0.4406	6.688	1.379
$B_{\delta_{lon}}$	-0.07667	6.934	0.8350
τ_{lon}	0.03099	16.40	5.196
τ_{lat}	0.03238	9.913	3.534
$cost_{\theta/\delta_{lon}}$		31.21546	
$cost_{q/\delta_{lon}}$		35.99568	
$cost_{p/\delta_{lon}}$		47.52514	
$cost_{\phi/\delta_{lat}}$		36.85730	
$cost_{q/\delta_{lat}}$		46.73137	
$cost_{p/\delta_{lat}}$		50.64457	
$cost_{total}$		41.4949	

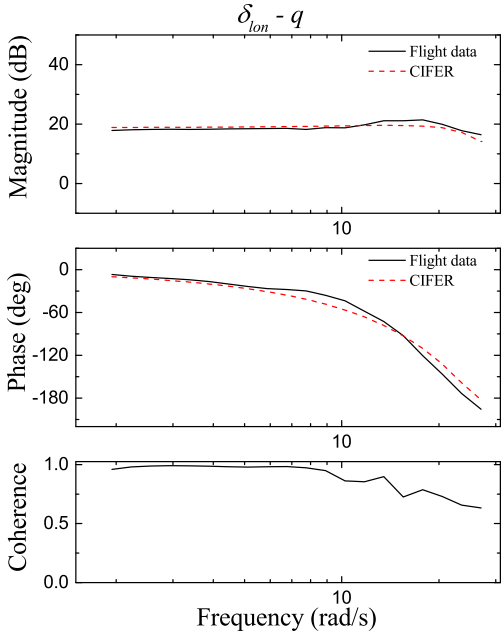

(a) δ_{lon}/q

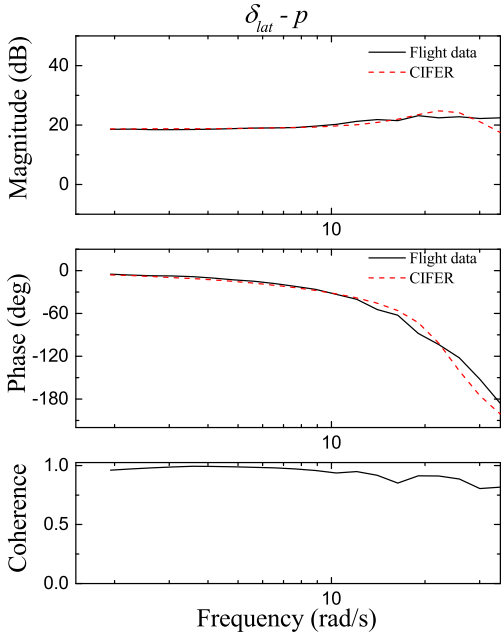

(b) δ_{lat}/p

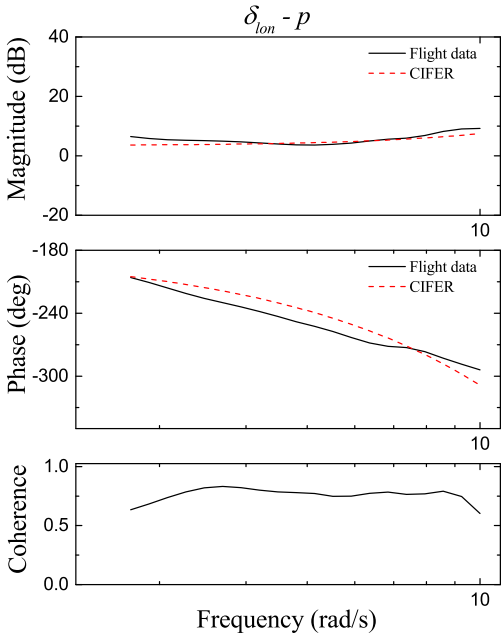

(c) δ_{lon}/p

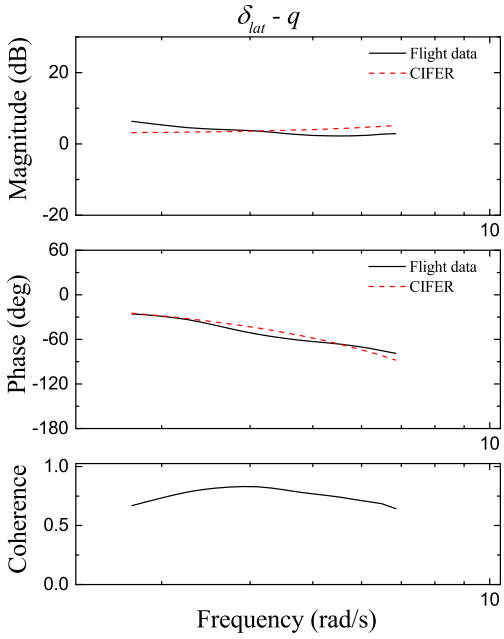

(d) δ_{lat}/q

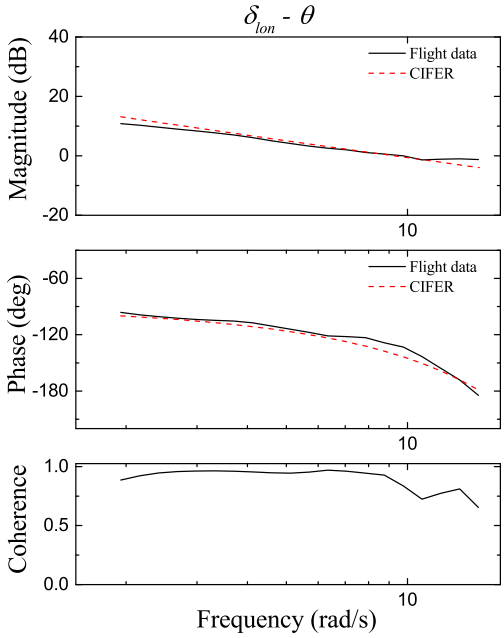

(e) δ_{lon}/θ

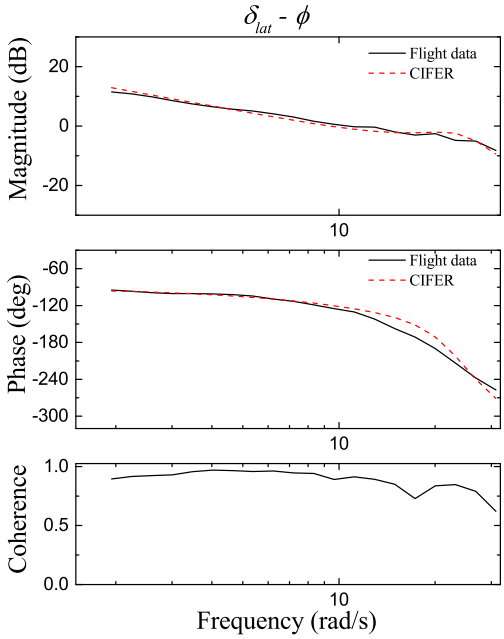

(f) δ_{lat}/ϕ

Figure 3. CIFER identification results in frequency domain.

4.2 Time domain results

For the time-domain PBSID$_{opt}$ method, among the 9 sets of flight data mentioned in Section 2, 5 sets are chosen for model identification, while the remaining 4 sets are used for cross validation. In the calculation, the singular values are shown in Figure 4. The first four points in the figure represent the low-frequency features of the rigid-body dynamics. During the identification, it is discovered that by adding 2 more states to the 4-order basic dynamics the identified PBSID$_{opt}$ model can be greatly improved with lower time-domain and frequency-domain errors. Thus, the model order is decided to be 6. In addition, p is decided equal to 13 and f is set equal to p. This decision is formed by several tries to acquire the best time-domain and frequency-domain performance in matching the flight responses.

Note that in system setting (Eq: 12), the incorrelation between u and w, v is not required, thus the PBSID$_{opt}$, unlike most other identification techniques, is feasible also for systems operating under feedback, just like the condition in Figure 2. The main-axis delay τ of the dynamics model is decided referring to the CIFER results.

The time-domain validation results are shown in Figures 6 and 7 in longitudinal and lateral directions. In the figures, the simulations of the angular velocity follow the original data well with small phase deviations. Apart from some errors in the peak value of the sweeps, the amplitude simulations have good accuracy. The calculations of θ and ϕ are basically good in following the original trends. There are small time delays discovered between the calculated θ and ϕ with the flight responses. In general, the PBSID$_{opt}$ method is successful in identifying the coupled roll/pitch model for the longitudinal and lateral time-domain responses.

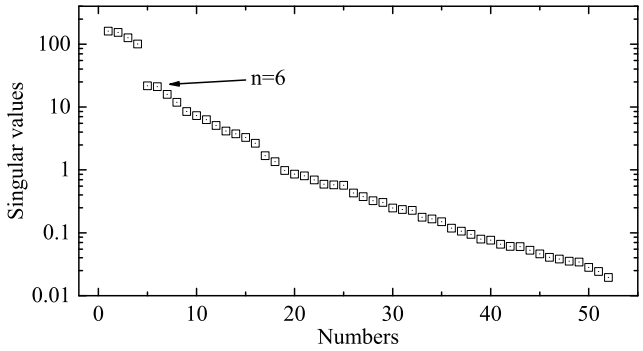

Figure 4. Singular values in PBSID$_{opt}$ calculation.

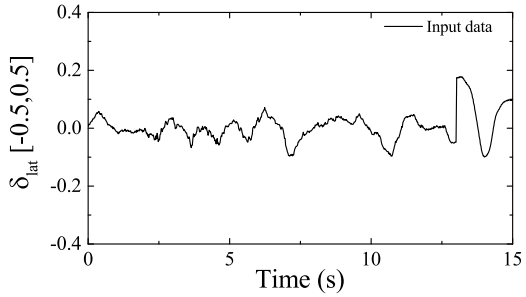

(a) δ_{lat}

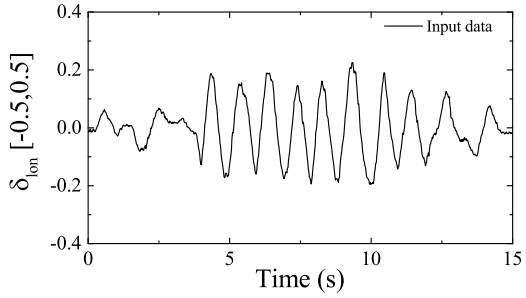

(b) δ_{lon}

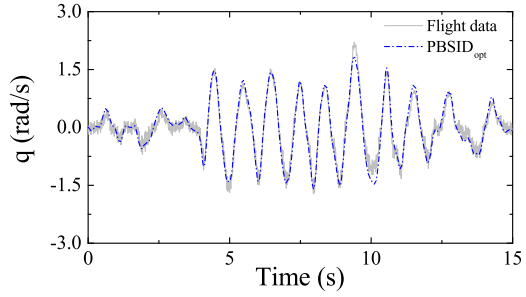

(c) q

4.3 Comparisons

Finally, Figures 8 and 9 show the time-domain comparisons of the PBSID$_{opt}$ model and the CIFER model. In q and p, there are tiny differences between the two models compared with the flight responses. In θ and ϕ, simulations in both models follow the original attitude angles in a satisfactory way. As time goes on, the attitude simulations of both models do not deviate from the original data greatly. Specifically note that simulations of the sweep amplitude of θ and ϕ by PBSID$_{opt}$ model are closer to the flight responses than the CIFER model.

In addition, the two models are compared in the frequency domain in Figure 10. The nonparametric frequency responses of the flight responses are ex-

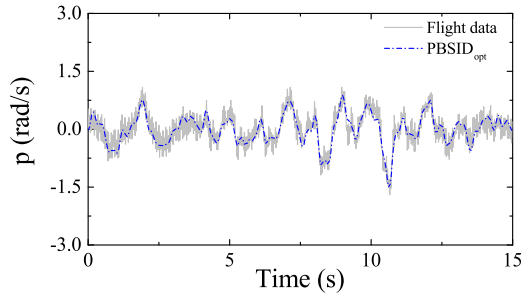

(d) p

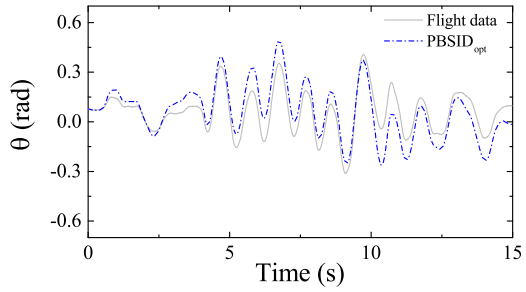

(e) θ

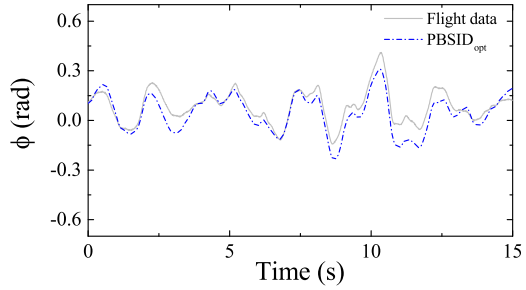

(f) ϕ

Figure 6. Longitudinal validations of PBSID$_{opt}$ in time domain.

ported by CIFER software, shown in the black lines. In channel δ_{lon}/q, CIFER and PBSID$_{opt}$ models give similar results on the magnitude and phase predictions. In low-frequency range below 3 rad/s, PBSID$_{opt}$ shows over prediction in phase. In channel δ_{lat}/p, both methods have similar frequency features below 15 rad/s, but above 15 rad/s, model of PBSID$_{opt}$ show closer results in phase but larger errors in magnitude to the nonparametric flight data. Similar to the main-axis angular velocity predictions, in δ_{lon}/θ, PBSID$_{opt}$ model shows over prediction in phase below 4 rad/s, and in δ_{lon}/ϕ, PBSID$_{opt}$ model shows more accurate results in phase but larger deviations in magnitude compared with CIFER model above 15 rad/s.

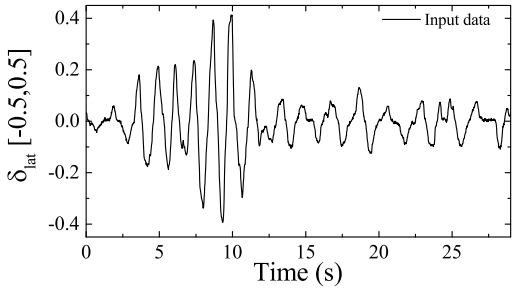

(a) δ_{lat}

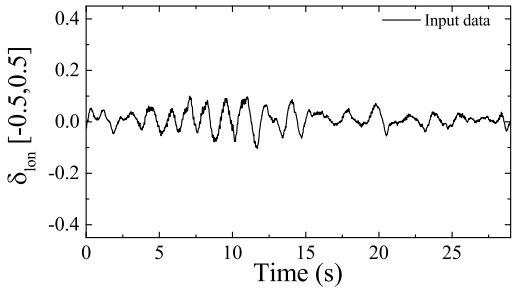

(b) δ_{lon}

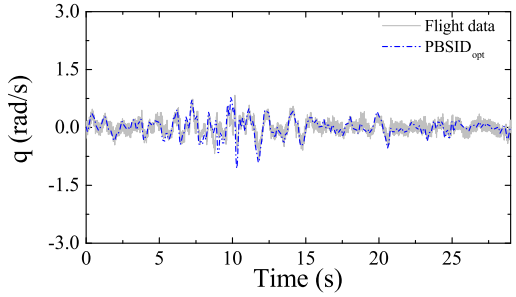

(c) q

In the off-axis responses (Figures 10 (e) and 10 (d)), CIFER and PBSID$_{opt}$ models have similar performances in predicting δ_{lat}/q, while in δ_{lon}/p, PBSID$_{opt}$ model shows larger deviations in magnitude and in low-frequency phase. Generally speaking, in the frequency domain, the CIFER model matches the flight responses better than the PBSID$_{opt}$ model. It is noteworthy that even if there are some underestimates by the PBSID$_{opt}$ model to predict on the high-frequency and off-axis responses, the time-domain validations show good results in simulating the attitude and angular velocities.

The eigenvalues of the two models are shown in Table 4. The eigenvalue positions show some differences between the two methods. Note that the two complex values of lateral and longitudinal modes dominate the identified dynamics, which are captured correctly by both methods.The small values represent the q/θ and p/ϕ

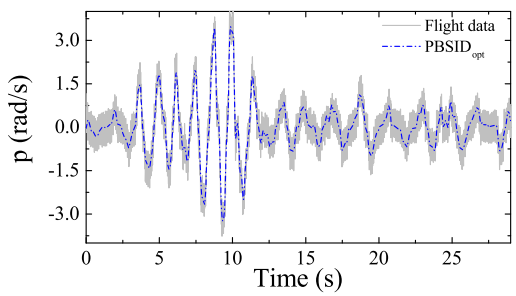

(d) p

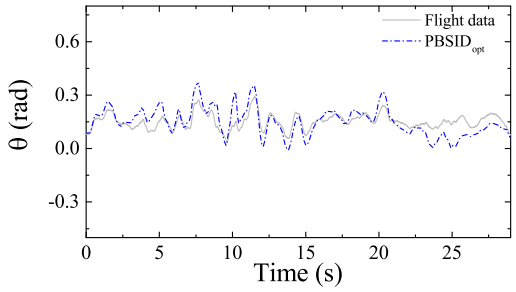

(e) θ

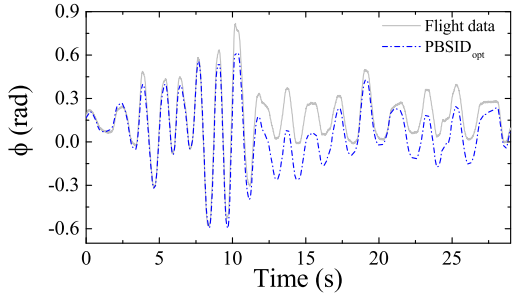

(f) ϕ

Figure 7. Lateral validations of PBSID$_{opt}$ in time domain.

responses. In the structured equation 5, these values are zero. The PBSID$_{opt}$ method is quite efficient and stable during calculations compared with the iterative CIFER method.

Table 4. Eigenvalue calculations.

	PBSID$_{opt}$	CIFER
lateral	$[-6.6480 \pm 17.9929i]$	$[-6.3760 \pm 23.3735i]$
longitudinal	$[-12.6193 \pm 10.1089i]$	$[-13.0953 \pm 16.0266i]$
small values	$[-0.6464 + 0i]$	$[0 + 0i]$
	$[-0.0861 + 0i]$	$[0 + 0i]$

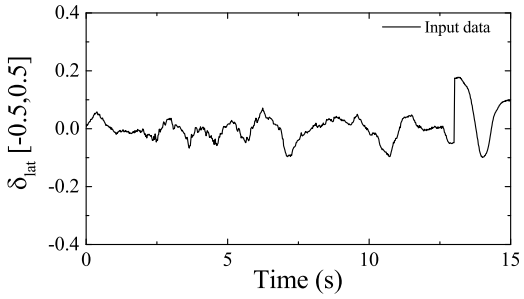

(a) δ_{lat}

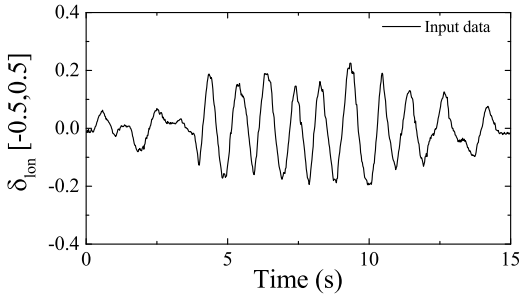

(b) δ_{lon}

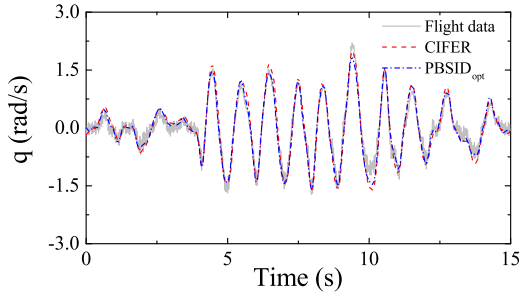

(c) q

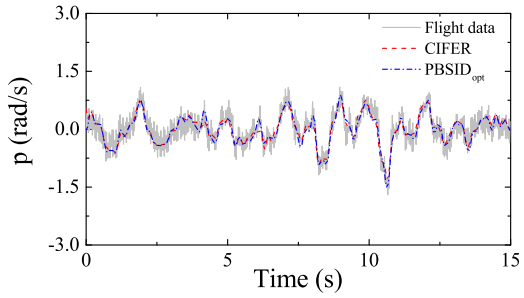

(d) p

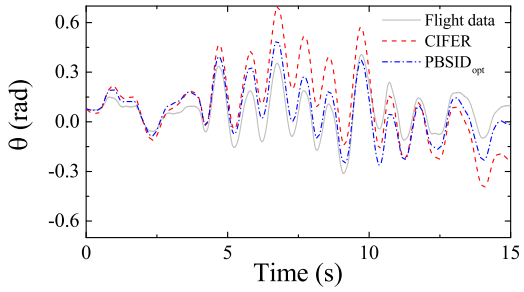

(e) θ

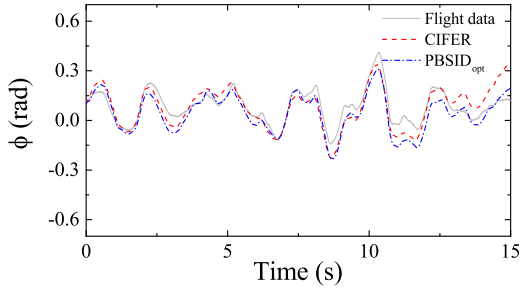

(f) ϕ

Figure 8. Longitudinal validations in time domain between CIFER and PBSID$_{opt}$.

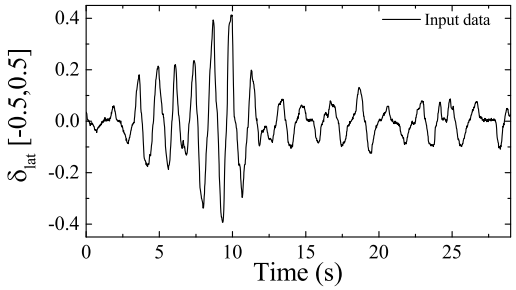

(a) δ_{lat}

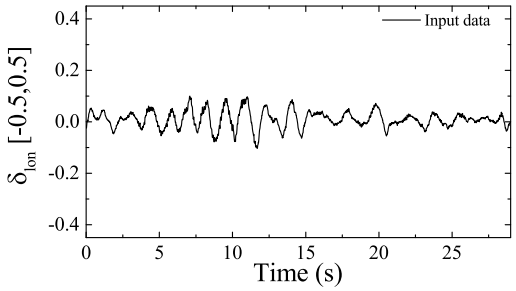

(b) δ_{lon}

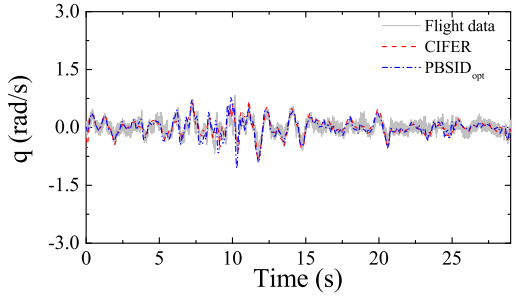

(c) q

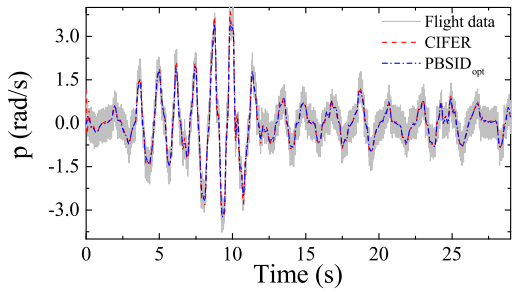

(d) p

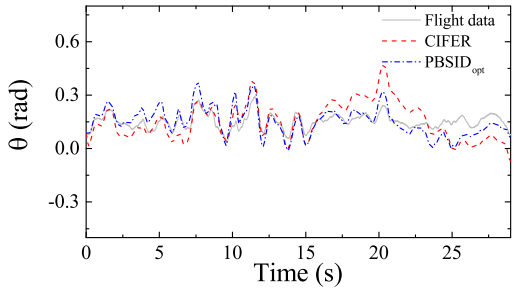

(e) θ

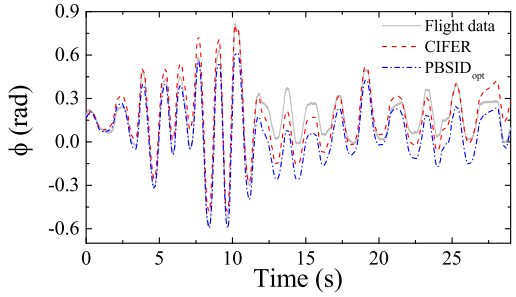

(f) ϕ

Figure 9. Lateral validations in time domain between CIFER and PBSID$_{opt}$.

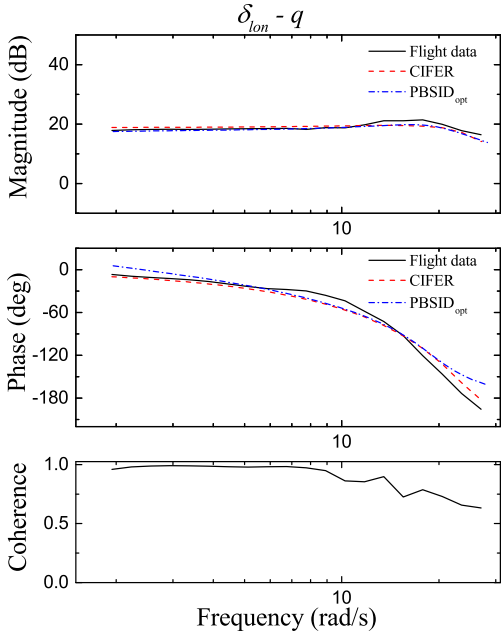

(a) δ_{lon}/q

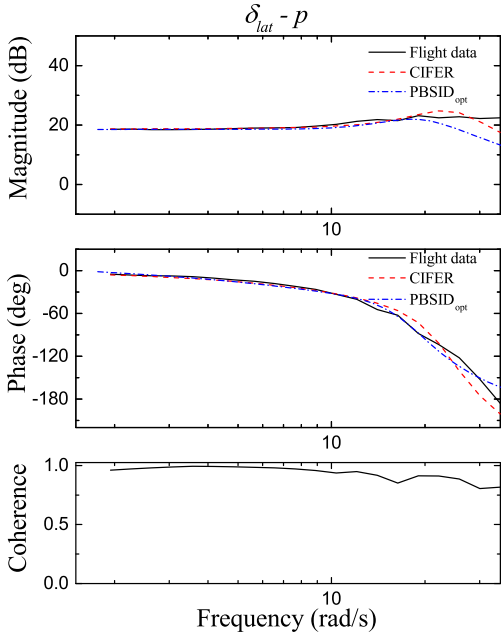

(b) δ_{lat}/p

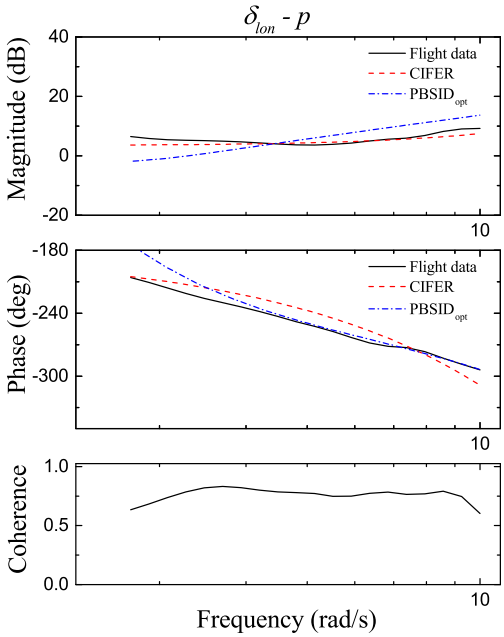

(c) δ_{lon}/p

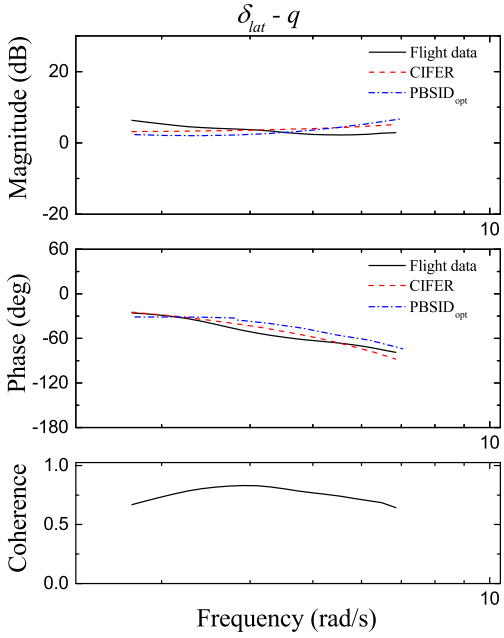

(d) δ_{lat}/q

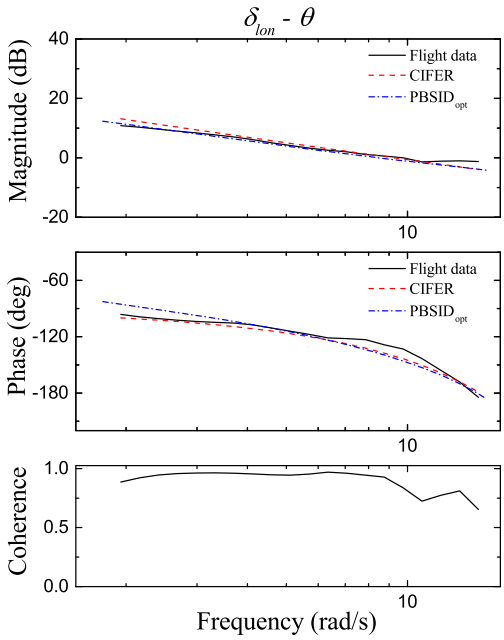

(e) δ_{lon}/θ

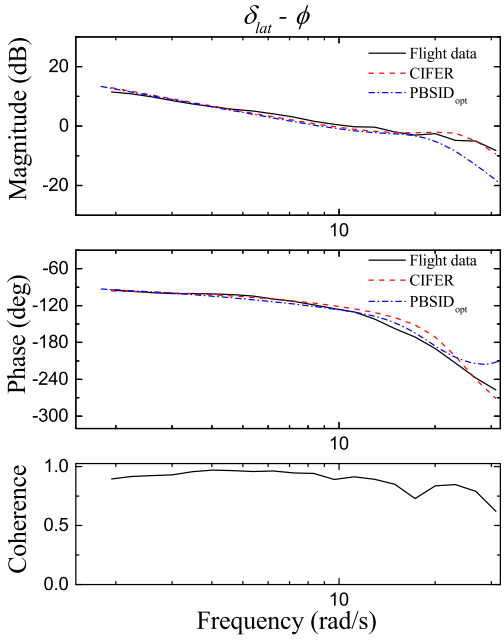

(f) δ_{lat}/ϕ

Figure 10. Comparisons between CIFER and PBSID$_{opt}$ in frequency domain.

5 Conclusions

In this work, the time-domain PBSID$_{opt}$ identification method and the frequency-domain CIFER one are considered in an identification problem of solving a coupled roll/pitch model of a small-scale helicopter. Both methods are successful in providing high-accuracy simulations of the time-domain responses, especially the angular velocity simulations. PBSID$_{opt}$ model simulates the θ and ϕ closer to the original data than CIFER. In frequency domain, both methods give good estimations in main-axis responses. In off-axis frequency predictions, CIFER model presents better results than PBSID$_{opt}$ model. Both methods capture the main dynamics modes of the coupled roll/pitch model in the eigenvalues. The model got from CIFER has physical meanings, while the model obtained by PBSID$_{opt}$ is non-structured. The process in PBSID$_{opt}$ has high efficiency and stability compared with in CIFER. Future work will be done to extract a structured model from the PBSID$_{opt}$ results.

References

[1] B Mettler, M B Tischler, and T Kanade. System identification modeling of a small-scale unmanned rotorcraft for flight control design. *Journal of the American helicopter society*, 47(1):50–63, 2002.

[2] F Yang, Z J Chen, and C Wei. Nonlinear system modeling and identification of small helicopter based on genetic algorithm. *International Journal of Intelligent Computing and Cybernetics*, 6(1):45–61, 2013.

[3] B Mettler. *Identification modeling and characteristics of miniature rotorcraft*. Springer Science & Business Media, 2013.

[4] B Mettler, V Gavrilets, and E Feron. Nonlinear model for a small-size acrobatic helicopter. In *AIAA Guidance, Navigation, and Control Conference and Exhibit*, page 4333, 2001.

[5] V Gavrilets, I Martinos, B Mettler, and E Feron. Control logic for automated aerobatic flight of a miniature helicopter. In *AIAA Guidance, Navigation, and Control Conference and Exhibit*, page 4834, 2002.

[6] S P Khaligh, F Fahimi, and C Robert Koch. A system identification strategy for nonlinear model of small-scale unmanned helicopters. *Journal of the American Helicopter Society*, 61(4):1–13, 2016.

[7] G W Cai, B M Chen, T H Lee, and K Y Lum. Comprehensive nonlinear modeling of an unmanned-aerial-vehicle helicopter. In *AIAA guidance, navigation and control conference and exhibit*, page 7414, 2008.

[8] S Bhandari and R Colgren. High-order dynamics models of a small uav helicopter using analytical and parameter identification techniques. *Journal of the American Helicopter Society*, 60(2):1–10, 2015.

[9] J Grauer, J Conroy, J Hubbard, J Humbert, and D Pines. System identification of a miniature helicopter. *Journal of Aircraft*, 46(4):1260–1269, 2009.

[10] R K Remple and M B Tischler. *Aircraft and rotorcraft system identification: engineering methods with flight-test examples*. American Institute of Aeronautics and Astronautics, 2006.

[11] P Van Overschee and B L De Moor. *Subspace identification for linear systems: Theory-Implementation-Applications*. Springer Science & Business Media, 2012.

[12] M Lovera. Identification of mimo state space models for helicopter dynamics. *IFAC Proceedings Volumes*, 36(16):1345–1350, 2003.

[13] M Verhaegen. Identification of the deterministic part of mimo state space models given in innovations form from input-output data. *Automatica*, 30(1):61–74, 1994.

[14] S Bittanti and M Lovera. Bootstrap-based estimates of uncertainty in subspace identification methods. *Automatica*, 36(11):1605–1615, 2000.

[15] L Ping and I Postlethwaite. Subspace and bootstrap-based techniques for helicopter model identification. *Journal of the American Helicopter Society*, 56(1):12002, 2011.

[16] M Bergamasco, A Ragazzi, and M Lovera. Rotorcraft system identification: a time/frequency domain approach. *IFAC Proceedings Volumes*, 47(3):8861–8866, 2014.

[17] M Bergamasco and M Lovera. Identification of linear models for the dynamics of a hovering quadrotor. *IEEE Transactions on Control Systems Technology*, 22(5):1696–1707, 2014.

[18] M Bergamasco and M Lovera. Continuous-time predictor-based subspace identification using laguerre filters. *IET Control Theory & Applications*, 5(7):856–867, 2011.

[19] A Chiuso. The role of vector autoregressive modeling in predictor-based subspace identification. *Automatica*, 43(6):1034–1048, 2007.

[20] G D Padfield. *Helicopter flight dynamics: the theory and application of flying qualities and simulation modelling*. John Wiley & Sons, 2008.

[21] A Chiuso. On the relation between cca and predictor-based subspace identification. *IEEE Transactions on Automatic Control*, 52(10):1795–1812, 2007.

[22] M F Weilenmann and H P Geering. A test bench for rotorcraft hover control. *Aiaa Journal*, 2013.